

Two-Dimensional Electron Gases at the Amorphous and Crystalline SrTiO₃/KTaO₃ Heterointerfaces

Hao Xu, Yulin Gan, Yuchen Zhao, Minghang Li, Xinzhe Hu, Xuanzhuang Chen, Ruwu Wang, Ying Li,* Jirong Sun, Fengxia Hu, Yunzhong Chen,* and Baogen Shen

The 5*d* two-dimensional electron gas (2DEG) based on KTaO₃ (KTO) exhibits a lot of exotic properties such as stronger spin-orbit coupling (SOC) and higher superconductivity transition temperature than those of SrTiO₃ (STO)-based 3*d* 2DEGs, whereas it has much lower electron mobility. Herein, the property of the 5*d* 2DEGs is investigated including the carrier mobility and Rashba SOC by interfacing both amorphous and crystalline STO with the crystalline KTO. Metallic 2DEGs are achieved at both interfaces of amorphous and crystalline STO-capped KTO. Notably, the amorphous STO/KTO heterointerface has a larger carrier concentration and higher Hall mobility than the crystalline STO/KTO counterparts at low temperatures, which stems from two kinds of carriers. In contrast, the 5*d* 2DEG formed at the crystalline interface exhibits much stronger Rashba SOC as revealed through magnetotransport measurement. The deduced maximum strength of Rashba SOC and spin-splitting energy are $\approx 8.56 \times 10^{-12}$ eV m and ≈ 33.52 meV, respectively. Our results provide new insights on designing on-demand properties of KTO-based conducting interfaces.

Complex oxide 2DEG was first found at the interface of two insulating nonmagnetic oxides LaAlO₃ (LAO) and SrTiO₃ (STO).^[1] Different from the 2DEG formed at traditional semiconductor interfaces like GaAs/AlGaAs, which are dominated by *s*- and *p*-orbital electrons,^[2] the 2DEGs produced at oxide interfaces such as LaAlO₃/SrTiO₃ (LAO/STO) are mainly derived from the strongly correlated 3*d* orbital electrons. The unique 2DEGs at oxide heterointerfaces have attracted much-renewed attention due to their particular properties, such as 2D superconductivity,^[3,4] magnetism,^[4–6] metal-insulator transition,^[7,8] quantum Hall effect,^[9] and tunable Rashba spin-orbit coupling,^[10,11] which arouse attracting huge interest for both fundamental and applied researches.^[1,12–14] Revealing the great potential of oxide interfaces with

1. Introduction

Designing on-demand functions for nanoscale devices is one of the major research directions of electronics. In this regard, controlling the low dimensional electron system, i.e., two-dimensional electron gas (2DEG) confined at the interface, and manipulating the charge and spin of carriers and their interconversion have great potential for spintronics.


strong electron correlations is expected to lead to new conceptual physics and applications.

The complex oxide 2DEG has been widely explored since 2004 besides LAO/STO interfaces, such as LaTiO₃/STO,^[15] LaVO₃/STO,^[16] NdGaO₃/STO, and CaZrO₃/STO.^[17,18] It is worth noticing that most of the previous works focused on STO-based 2DEGs, where the electrons come from the Ti 3*d* *t*_{2g} orbitals electrons residing in STO. Apart from SrTiO₃, KTaO₃ (KTO) is a promising substrate of 5*d* transition-metal oxide, which can also produce 2DEGs with characteristics of 5*d*-orbitals, for example, on the Ar⁺ ions irradiating of KTO surface,^[19] or at the interface between the LaAlO₃,^[20–22] LaVO₃,^[23] LaTiO₃,^[24] EuO or Al₂O₃ overlayers and KTaO₃.^[25,26] KTO has the same high permittivity as STO, but its spin-orbit coupling (SOC) is 20 times stronger than STO.^[27,28] Different from STO-based 3*d* 2DEG, the 5*d* 2DEG based on KTO exhibits a lot of exotic properties such as stronger Rashba spin-orbit coupling and higher superconductivity transition temperature.^[20,26,29,30]

Moreover, the physical properties of the 5*d* 2DEGs can also be tunable by the external stimuli, like electric gating,^[30,31] ionic or light irradiation.^[20,26,32,33] It has also been indicated that the 5*d* 2DEG possesses a lower electron mobility than the typical 1000 cm² V⁻¹ s⁻¹ at 2 K for STO-based 2DEGs.^[21,25,26] Therefore, much more work needs to be done to fully explore the KTO-based 2DEG and the effect of capping layer as well as interface engineering on interfacial carriers' property. Additionally, the strong Rashba SOC is one of the most attractive

H. Xu, X. Chen, R. Wang, Y. Li
The State Key Laboratory of Refractories and Metallurgy
Hubei Province Key Laboratory of Systems Science in Metallurgical Process
Collaborative Innovation Center for Advanced Steels
International Research Institute for Steel Technology
Faculty of Science
Wuhan University of Science and Technology
Wuhan, Hubei 430065, China
E-mail: liying89@wust.edu.cn

H. Xu, Y. Gan, Y. Zhao, M. Li, X. Hu, J. Sun, F. Hu, Y. Chen, B. Shen
Beijing National Laboratory of Condensed Matter Physics and Institute of Physics
Chinese Academy of Sciences
Beijing 100190, China
E-mail: yzchen@iphy.ac.cn

 The ORCID identification number(s) for the author(s) of this article can be found under <https://doi.org/10.1002/pssa.202300235>.

DOI: 10.1002/pssa.202300235

features in KTO-based $5d$ 2DEG. It is also interesting to determine the effect of capping layer on the SOC with respect to spintronic applications.

In this work, we successfully created metallic interfaces of STO/KTO, by tuning the crystalline state of the STO capping layer. 2DEGs with distinct carrier types and behaviors were achieved at both the amorphous and crystalline STO/KTO heterointerfaces, respectively. The most interesting observation is that the 2DEG at amorphous-STO/KTO (a-STO/KTO) heterogeneous interface possesses higher carrier concentration and Hall mobility than that at crystalline-STO/KTO (c-STO/KTO) interface at low temperatures, which may stem from two kinds of carriers. In contrast, the 2DEG at c-STO/KTO heterointerface exhibits much stronger Rashba SOC effect.

2. Results and Discussion

Both amorphous and crystalline STO films (a-STO, c-STO) are fabricated on single-crystal (001)-KTO substrates by pulsed laser deposition (PLD) method, at 25 and 650 °C under limited vacuum pressures, which are $\approx 1 \times 10^{-7}$ mbar at 25 °C and $\approx 1 \times 10^{-6}$ mbar at 650 °C, respectively. Previous research shows no dependence of the interfacial conduction on the pressure in this range ($\approx 1 \times 10^{-7} - \approx 1 \times 10^{-6}$ mbar) for KTO-based 2DEG. **Figure 1a** illustrates the atomic schematic structures of a-STO/KTO and c-STO/KTO heterointerfaces, given that the lattice mismatch between STO and KTO is 2.1%. The growth of amorphous and crystalline STO capping films is monitored in situ by the reflection high energy electron diffraction (RHEED) as depicted in Figure S1a,b, Supporting Information, and the structure is further confirmed by the XRD patterns. For the sample prepared at room temperature, only the peaks of KTO single-crystal substrate are detected (Figure 1b) without any Bragg reflections of STO, confirming the amorphous structure of STO layer. While clear Bragg (002) reflections of STO can be observed in c-STO/KTO epitaxially grown at 650 °C (Figure 1d). The thickness of STO upper films is ≈ 10 nm as deduced by the fitting curves of small-angle X-ray reflectivity (XRR) (Figure 1c,e). It is found that the roughness of STO capping films will be affected by the polar KTO surface during growth because of oxygen vacancy and volatilization of potassium, while does not affect the existence of 2DEG (Figure S1–S3, Supporting Information).

As shown in **Figure 2a**, the STO/KTO samples are patterned with Hall Bar (50 μm in width and 500 μm in length) using standard optical lithography and lift-off techniques 200 nm thick AlO_x films as the hard mask.^[30] The temperature dependence of the sheet resistance (R_s) in Figure 2b suggests metallic conduction at both a-STO/KTO and c-STO/KTO interfaces over the temperature range from 2 to 300 K. It is worth noting that the $R_s(300\text{ K})/R_s(2\text{ K})$ ratio of c-STO/KTO is ≈ 9 , which is around sixfold lower than that of a-STO/KTO (≈ 56), implying a better metallic character of the 2DEG at a-STO/KTO. Notably, in Figure 2c, the nonlinear Hall resistance behavior is observed for 2DEG at a-STO/KTO from 2 to 30 K, where the linear Hall resistance ($R_{xy}-B$) at low field is followed by a transition to nonlinear at high field. By contrast, the Hall resistance ($R_{xy}-B$) displays well linear variation up to 12 T with a negative

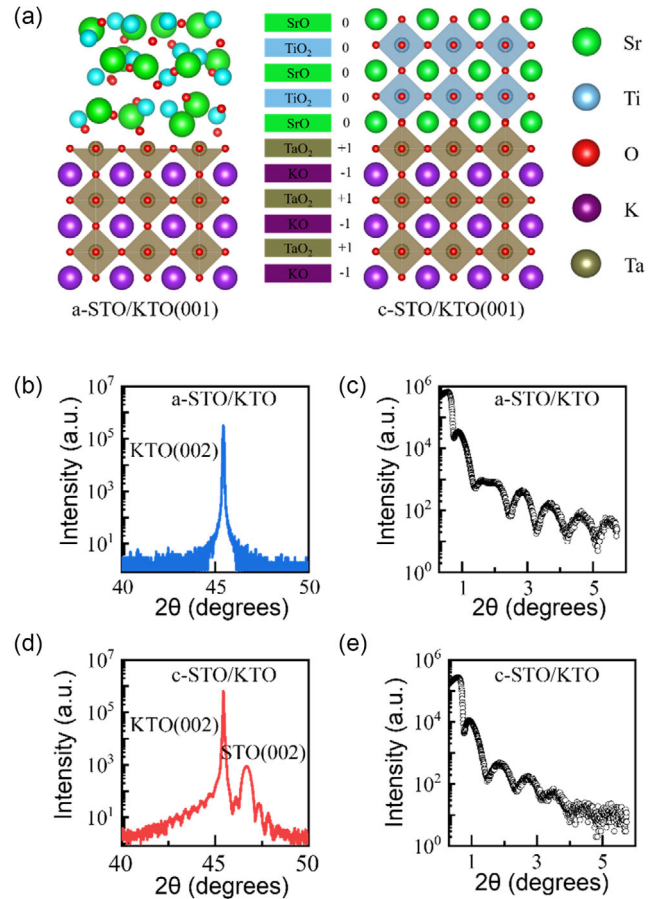


Figure 1. a) The crystal structure of the two STO/KTO heterostructures. b,d) The XRD 2θ - ω scan around the KTO (002) peak of the two STO/KTO heterostructures. c,e) Small-angle X-ray reflectivity spectrum of the two STO films. The thicknesses of the thin films are obtained according to curve fitting.

slope at the c-STO/KTO interface (Figure 2d), indicating only one single carrier contributing to the 2DEG. The Hall coefficient changes negligibly with respect to cooling and warming, implying that the carrier density hardly changes with temperature.

The nonlinear Hall behavior ($R_{xy}-B$) of the a-STO/KTO 2DEG reveals that there are two-type charge carriers contributing to the transport properties.^[34] The mobility and density of the two kinds of charge carriers are analyzed and deduced by fitting the experimental data $R_{xy}(B)$, using the two-band model^[15,34–36]

$$R_{xy}(B) = \frac{1}{e} \frac{\left(\frac{n_1 \mu_1^2}{1 + \mu_1^2 B^2} + \frac{n_1 \mu_1^2}{1 + \mu_2^2 B^2} \right) B}{\left(\frac{n_1 \mu_1^2}{1 + \mu_1^2 B^2} + \frac{n_1 \mu_1^2}{1 + \mu_2^2 B^2} \right)^2 + \left(\frac{n_1 \mu_1^2}{1 + \mu_1^2 B^2} + \frac{n_1 \mu_1^2}{1 + \mu_2^2 B^2} \right)^2 B^2} \quad (1)$$

with the constraint of

$$R_s(0) = \frac{1}{e(n_1 \mu_1 + n_2 \mu_2)} \quad (2)$$

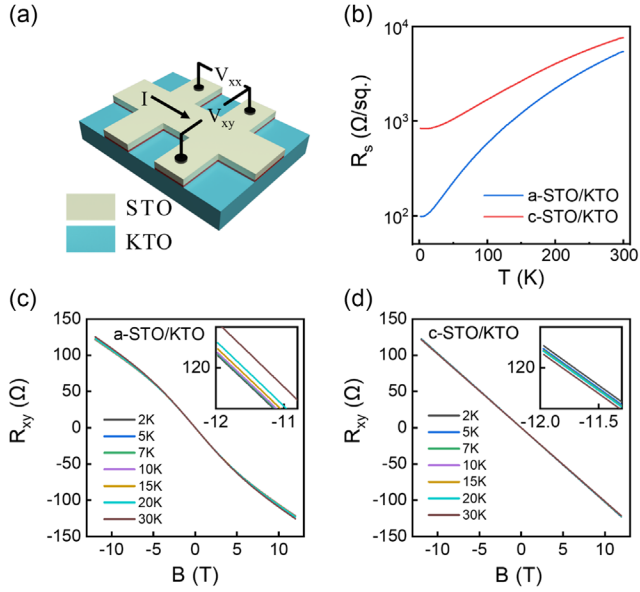


Figure 2. a) Schematic of the standard STO/KTO device with Hall Bar geometry for transport measurements. b) Temperature dependence of the sheet resistance for the 2DEGs formed at the two STO/KTO hetero-interfaces, measured from 2 to 300 K. c) and d) Hall resistance (R_{xy}) of the 2DEGs in a-STO/KTO and c-STO/KTO, measured from -12 to 12 T under different temperatures. The insets are the larger version of (c) and (d).

where n_1 and n_2 denote, respectively, the density of the two species of charge carriers, and μ_1 , μ_2 are the corresponding Hall mobility. For 2DEG at the a-STO/KTO interface, the temperature dependence of the two types of carriers' densities n_1 , n_2 are shown in Figure 3a. As temperatures rise from 2 to 50 K, the density of carriers decreases from $n_1 \approx 1.66 \times 10^{13}$ to $\approx 0.72 \times 10^{13} \text{ cm}^{-2}$ and $n_2 \approx 5.73 \times 10^{13}$ to $\approx 5.71 \times 10^{13} \text{ cm}^{-2}$, and the mobility of charge carriers changes from $\mu_1 \approx 2118$ to $\approx 1156 \text{ cm}^2 (\text{V s})^{-1}$ and $\mu_2 \approx 496$ to $\approx 341 \text{ cm}^2 (\text{V s})^{-1}$. The total carrier density n_a ($n_a = n_1 + n_2$) decreases from $\approx 7.37 \times 10^{13}$ to $\approx 6.45 \times 10^{13} \text{ cm}^{-2}$, mainly affected by carriers of type I (n_1). Above 50 K, there is only one species of charge carrier existing. In total, an 87% enhancement in n_a takes place from $n_a = 3.9 \times 10^{13} \text{ cm}^{-2}$ (300 K) to $n_a = 7.3 \times 10^{13} \text{ cm}^{-2}$ at 2 K. Different from the a-STO/KTO interface, the carrier density n_c for the c-STO/KTO 2DEG shows temperature independence ($\approx 6.1 \times 10^{13} \text{ cm}^{-2}$), and such feature was only observed at the crystalline LAO/STO interface before.^[1] The Hall mobility (μ) of 2DEGs is shown in Figure 3b for both a-STO/KTO and c-STO/KTO, which exhibits the power law temperature dependence similar to that at LAO/STO interface, due to the electron scattering by optical phonons. It is intriguing that the a-STO/KTO 2DEG has the Hall mobility of $402 \text{ cm}^2 (\text{V s})^{-1}$ at 2 K, which is more than three times higher than that ($\approx 122 \text{ cm}^2 (\text{V s})^{-1}$) of c-STO/KTO 2DEG.

As for oxide 2DEG, the linear-to-nonlinear Hall resistance behavior means the occurrence of Lifshitz transition. When the carrier density exceeds the Lifshitz transition point, SOC decreases rapidly. In Figure 2c,d, the Hall resistance of a-STO/KTO 2DEG is nonlinear while that of c-STO/KTO 2DEG is linear at 2 K. Therefore, we conclude that the Lifshitz

transition point n_s in the STO/KTO 2DEG system is between 6.1×10^{13} and $7.37 \times 10^{13} \text{ cm}^{-2}$. The carrier density n_s of c-STO/KTO at 2 K closes to the Lifshitz transition point, so c-STO/KTO 2DEG shows strong the Rashba SOC effect, and the carrier density n_s of a-STO/KTO at 2 K is much higher than the Lifshitz transition point, so its Rashba SOC is very weak. In contrast, we have retested the electrical transport properties of 2DEG in a-STO/KTO sample after 3 months, and we found its carrier density n_s decreases to $2.7 \times 10^{13} \text{ cm}^{-2}$ at 2 K (See Figure S4, Supporting Information), which is far less than the Lifshitz transition point. Thus, the Hall resistance becomes linear and the Rashba SOC is very weak, which further prove that the conclusion is correct. Figure 3c,d shows the magnetoresistance (MR) with respect to magnetic field for the $5d$ 2DEGs from 2 to 30 K, where MR is defined as $[R(B) - R(0)]/R(0)$.^[26] Notably, at low temperatures, the MR- B curves of the c-STO/KTO 2DEG exhibit a clear cusp around $B = 0$, which is the typical feature of weak antilocalization (WAL) of 2DEG, as for amorphous, its magnetic resistance is strongly modified by the dual carriers of 2DEG, which makes the WAL signal hardly to be identified. With the temperature increasing, the cusp around $B = 0$ becomes broad and gradually disappears for that the WAL effect is weakening. Here, the WAL originates from the quantum interference of the coherent electronic waves in the WAL system with Rashba SOC, where the SOC suppresses quantum backscattering-induced WAL, leading to the prominent WAL.^[10,37] Based on the literatures,^[10,38] we employ the Maekawa-Fukuyama (MF) theory to analyze the WAL of c-STO/KTO 2DEG at the normal state and quantitatively derive the spin-orbit term B_{so} . Three characteristic magnetic fields [$B_k = \hbar/(4eD\tau_k)$, $k = e, i$, so] are introduced to characterize B -dependent quantum correction of three scattering processes,^[38] where, τ_e , τ_i , and τ_{so} are the elastic scattering time, the inelastic scattering time, and the spin-orbit scattering time, respectively. $D = v_F^2\tau_e/2$ is the diffusion constant given by the Drude model. On the basis of the MF formula, the relationship of the first-order quantum correction of WAL and the classical magnetoconductance is analyzed, and the correction to the total magnetoconductance can be expressed as^[10]

$$\begin{aligned} \frac{\Delta\sigma_{xx}(B)}{G_0} = & -\psi\left(\frac{1}{2} + \frac{B_e + B_{so}}{B}\right) + \psi\left(\frac{1}{2} + \frac{B_i + B_{so}}{B}\right) \\ & + \frac{1}{2}\psi\left(\frac{1}{2} + \frac{B_i + 2B_{so}}{B}\right) - \frac{1}{2}\psi\left(\frac{1}{2} + \frac{B_i}{B}\right) \\ & - \left[\ln\left(\frac{B_i + B_{so}}{B_e + B_{so}}\right) + \frac{1}{2}\ln\left(\frac{B_i + 2B_{so}}{B_i}\right) \right] - A_k \frac{\sigma_{xx}(0)}{G_0} \frac{B^2}{1 + CB^2} \end{aligned} \quad (3)$$

Here, the $\psi(x)$ is the digamma function. The parameters A_k and C from the last term describe the classical magnetoconductance, and $G_0 = e^2/\pi h$ is a universal value of conductance. As shown in Figure 4a, the fitting curves of normalized magnetoconductance fit well with the experimental data according to the Maekawa-Fukuyama theory for 2DEG in c-STO/KTO. Figure 4b demonstrates the deduced SOC characteristic field B_{so} as the functions of temperature, which decreases from ≈ 1.07 to 0.45 T as temperature rises. The strength of the Rashba SOC is related to the fitted inverse spin relaxation length q_{so} through $\alpha_R = \hbar^3 q_{so}/2m^*$, where the α_R is Rashba coefficient,

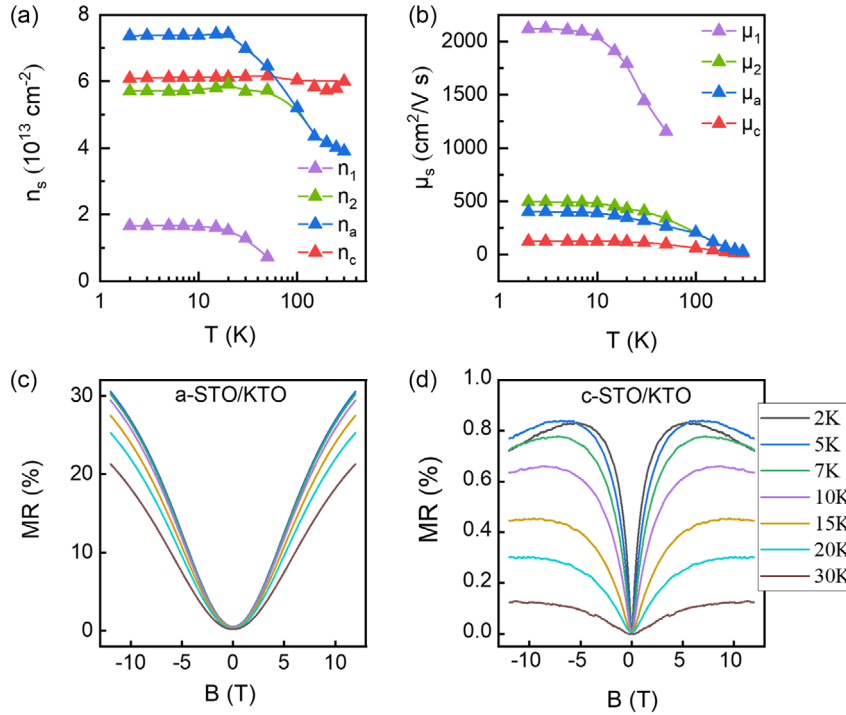


Figure 3. a,b) The corresponding carrier density (n_1 , n_2 , n_a , and n_c) and Hall mobility (μ_1 , μ_2 , μ_a , and μ_c) for each species of charge carriers in the a-STO/KTO and c-STO/KTO 2DEGs, as functions of temperature. c,d) The magnetoresistance (MR) of a-STO/KTO and c-STO/KTO 2DEGs at low temperatures.

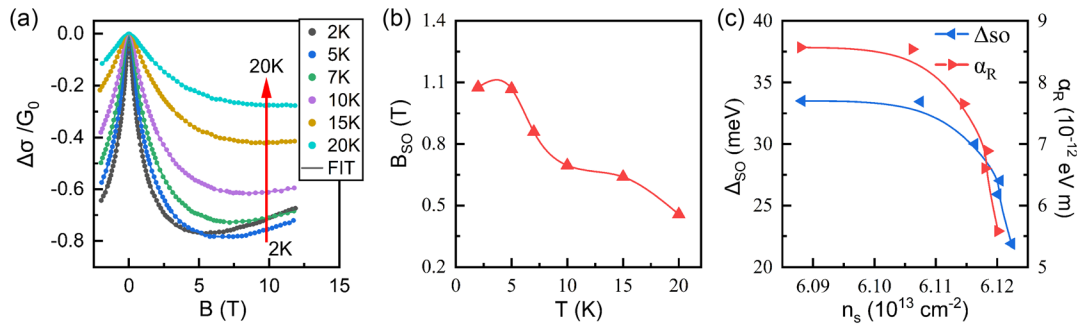


Figure 4. a) The fitting of normalized magnetoconductance according to the Maekawa–Fukuyama theory for 2DEGs in c-STO/KTO. b) The deduced SOC characteristic field B_{SO} as functions of temperature. c) The deduced spin splitting energy Δ_{SO} and the strength of Rashba coefficient α_R as a function of carrier density for c-STO/KTO 2DEGs.

and the m^* is the effective mass of the electrons,^[39] which is $0.36 m_e$ for KTO $5d$ 2DEG,^[24] much less than that of STO.^[10] The spin relaxation length q_{SO} can be calculated using $q_{SO} = (D\tau_{SO})^{-\frac{1}{2}}$.^[39] The spin-orbit effective field B_{SO} is defined as $B_{SO} = \hbar/4eD\tau_{SO}$. Thus, the strength of the Rashba SOC α_R can be obtained as $\alpha_R = \frac{\sqrt{e\hbar^3 B_{SO}}}{m^*}$, where the B_{SO} can be extracted by the MR curves fitting. The spin-splitting energy is given by $\Delta_{SO} = 2\alpha_R k_F$, in which the k_F is the Fermi wave vector, and $k_F = \sqrt{2\pi n_s}$.^[10] Figure 4c summarizes the spin splitting energy Δ_{SO} and Rashba coefficient α_R as a function of the carrier density, demonstrating that the maximum Δ_{SO} and α_R are $\approx 33.52 \text{ meV}$ and $\approx 8.56 \times 10^{-12} \text{ eV m}$, respectively. The spin split energy is comparable to that of the amorphous-LAO/KTO and GAO/KTO heterostructure,^[20,26] but larger than that of STO-based 2DEG as expected.^[10,11,40–42]

3. Conclusion

In conclusion, we have created two types of metallic oxide interfaces by interfacing both amorphous and crystalline STO capping layers with the polar substrate KTO. Metallic $5d$ 2DEGs are achieved in both cases. Notably, the amorphous STO/KTO heterointerface possesses larger carrier concentration and higher Hall mobility than that in the crystalline STO/KTO counterparts at low temperatures. There are two types of carriers in the 2DEG of a-STO/KTO below 50 K, and the same phenomena are observed at the a-LaAlO₃/KTO interface. The band structure of KTO surface is similar to the LAO/STO case with the parabolic dispersion relation, in which the Rashba splitting results in the shift of d_{xz}/d_{yz} bands. In this scenario, the mobile electrons will first occupy the low-level d_{xy} states near KTO surface, and then fill into the d_{xz}/d_{yz} orbitals when the carrier density increases and

Fermi energy approaches a threshold value, generating two different carriers in the a-STO/KTO. The 2DEG formed at crystalline STO/KTO heterointerface is relatively stable with the carrier of a single kind, and exhibits strong Rashba spin-orbit coupling effect at low temperatures, in which the maximum spin-orbit characteristic magnetic field B_{so} and spin splitting energy Δ_{SO} can be up to ≈ 1.07 T and ≈ 33.52 meV, respectively. It is noticed that defects like oxygen vacancies and potassium vacancies would have serious impacts on the polar KTO surface and the complex interface during high-temperature growth (Figure S2 and S3, Supporting Information), which could influence the high-quality of the 2DEGs that originate mainly from the oxygen vacancies in KTO surface, and thus the mobility of carriers is much different for samples grown at different temperatures. Our work presents important information on the design of the physical properties of the $KTaO_3$ -based $5d$ 2DEG.

4. Experimental Section

Both amorphous and crystalline STO films were fabricated on single-crystal (001)-KTO substrates ($5 \times 5 \times 0.5$ mm³) in pulsed laser deposition (PLD) system with a 248-nm KrF excimer laser (1.5 J cm⁻², 2 Hz), while varying the temperature at 25 and 650 °C under limited vacuum pressure, respectively. Samples are furnace-cooled to room temperature at on-site oxygen pressure after deposition. The surface morphology of the film was analyzed by atomic force microscopy (AFM, Bruker MultiMode8) at the ambient conditions. The crystal structure and thickness (≈ 10 nm) of the films were determined by X-ray diffraction and X-ray reflectivity, respectively (Bruker D8 Discover, Cu K α radiation). Magnetotransport measurements were performed on Hall Bar samples by quantum-design physical property measurement system (PPMS) with temperature from 2 to 300 K and magnetic field up to 12 T. Ultrasonic bonded Al wire of 20 μ m in diameter was used as electrode contact.

Supporting Information

Supporting Information is available from the Wiley Online Library or from the author.

Acknowledgements

This work was financially supported by the National Natural Science Foundation of China (grant nos. 11704292 and 12204523), the Science Center of the National Science Foundation of China (52088101), the National Key Research and Development Program of China (2021YFA1400300), the National Science Foundation of Hubei Province (2017CFB148), and Wuhan Science and Technology Association (Wuhan Youth Science and Technology Sunrise Plan, No. whkx202201). Yulin Gan also acknowledges the support from China Postdoctoral Science Foundation (2020M680726 and YJ20200325). [Correction added on 07 July 2023 after initial publication: In Figure 4 panel (c), the order of magnitude for α_R was corrected from " 10^{12} eVm" to " 10^{-12} eVm".]

Conflict of Interest

The authors declare no conflict of interest.

Data Availability Statement

The data that support the findings of this study are available from the corresponding author upon reasonable request.

Keywords

5d two-dimensional electron gas, amorphous interfaces, electronic transport, $KTaO_3$, Rashba spin-orbit coupling

Received: March 30, 2023
Published online: May 31, 2023

- [1] A. Ohtomo, H. Y. Hwang, *Nature* **2004**, *427*, 423.
- [2] R. Winkler, *Spin-Orbit Coupling Effects in Two-Dimensional Electron and Hole Systems*, Springer, Berlin; New York **2003**.
- [3] N. Reyren, S. Thiel, A. D. Caviglia, L. F. Kourkoutis, G. Hammerl, C. Richter, C. W. Schneider, T. Kopp, A.-S. Rüetschi, D. Jaccard, M. Gabay, D. A. Muller, J.-M. Triscone, J. Mannhart, *Science* **2007**, *317*, 1196.
- [4] D. A. Dikin, M. Mehta, C. W. Bark, C. M. Folkman, C. B. Eom, V. Chandrasekhar, *Phys. Rev. Lett.* **2011**, *107*, 056802.
- [5] A. Brinkman, M. Huijben, M. van Zalk, J. Huijben, U. Zeitler, J. C. Maan, W. G. van der Wiel, G. Rijnders, D. H. A. Blank, H. Hilgenkamp, *Nat. Mater.* **2007**, *6*, 493.
- [6] D. Stornaiuolo, C. Cantoni, G. M. De Luca, R. Di Capua, E. Di Gennaro, G. Ghiringhelli, B. Jouault, D. Marrè, D. Massarotti, F. Miletto Granozio, I. Pallecchi, C. Piamonteze, S. Rusponi, F. Tafuri, M. Salluzzo, *Nat. Mater.* **2016**, *15*, 278.
- [7] C. Cen, S. Thiel, G. Hammerl, C. W. Schneider, K. E. Andersen, C. S. Hellberg, J. Mannhart, J. Levy, *Nat. Mater.* **2008**, *7*, 298.
- [8] P. P. Aurino, A. Kalabukhov, N. Tuzla, E. Olsson, A. Klein, P. Erhart, Y. A. Boikov, I. T. Serenkov, V. I. Sakharov, T. Claesson, D. Winkler, *Phys. Rev. B* **2015**, *92*, 155130.
- [9] F. Trier, G. E. D. K. Prawiroatmodjo, Z. Zhong, D. V. Christensen, M. von Soosten, A. Bhowmik, J. M. G. Lastra, Y. Chen, T. S. Jespersen, N. Pryds, *Phys. Rev. Lett.* **2016**, *117*, 096804.
- [10] A. D. Caviglia, M. Gabay, S. Gariglio, N. Reyren, C. Cancellieri, J.-M. Triscone, *Phys. Rev. Lett.* **2010**, *104*, 126803.
- [11] G. Herranz, G. Singh, N. Bergeal, A. Jouan, J. Lesueur, J. Gázquez, M. Varela, M. Scigaj, N. Dix, F. Sánchez, J. Fontcuberta, *Nat. Commun.* **2015**, *6*, 6028.
- [12] N. Nakagawa, H. Y. Hwang, D. A. Muller, *Nat. Mater.* **2006**, *5*, 204.
- [13] G. Herranz, M. Basletić, M. Bibes, C. Carrétéro, E. Tafrá, E. Jacquet, K. Bouzehouane, C. Deranlot, A. Hamzić, J.-M. Broto, A. Barthélémy, A. Fert, *Phys. Rev. Lett.* **2007**, *98*, 216803.
- [14] A. D. Caviglia, S. Gariglio, C. Cancellieri, B. Sacépé, A. Fête, N. Reyren, M. Gabay, A. F. Morpurgo, J.-M. Triscone, *Phys. Rev. Lett.* **2010**, *105*, 236802.
- [15] J. S. Kim, S. S. A. Seo, M. F. Chisholm, R. K. Kremer, H.-U. Habermeier, B. Keimer, H. N. Lee, *Phys. Rev. B* **2010**, *82*, 201407.
- [16] Y. Hotta, T. Susaki, H. Y. Hwang, *Phys. Rev. Lett.* **2007**, *99*, 236805.
- [17] F. Gunkel, K. Skaja, A. Shkabko, R. Dittmann, S. Hoffmann-Eifert, R. Waser, *Appl. Phys. Lett.* **2013**, *102*, 071601.
- [18] L. Chen, J. Li, Y. Tang, Y.-Y. Pai, Y. Chen, N. Pryds, P. Irvin, J. Levy, *Adv. Mater.* **2018**, *30*, 1801794.
- [19] S. Harashima, C. Bell, M. Kim, T. Yajima, Y. Hikita, H. Y. Hwang, *Phys. Rev. B* **2013**, *88*, 085102.
- [20] H. Zhang, X. Yan, X. Zhang, S. Wang, C. Xiong, H. Zhang, S. Qi, J. Zhang, F. Han, N. Wu, B. Liu, Y. Chen, B. Shen, J. Sun, *ACS Nano* **2019**, *13*, 609.
- [21] H. Zhang, X. Yan, J. Zhang, J. Zhang, F. Han, H. Huang, S. Qi, W. Shi, B. Shen, J. Sun, *Mater. Res. Express* **2019**, *6*, 086448.
- [22] H. Zhang, H. Zhang, X. Yan, X. Zhang, Q. Zhang, J. Zhang, F. Han, L. Gu, B. Liu, Y. Chen, B. Shen, J. Sun, *ACS Appl. Mater. Interfaces* **2017**, *9*, 36456.

- [23] N. Wadehra, R. Tomar, R. M. Varma, R. K. Gopal, Y. Singh, S. Dattagupta, S. Chakraverty, *Nat. Commun.* **2020**, *11*, 874.
- [24] K. Zou, S. Ismail-Beigi, K. Kisslinger, X. Shen, D. Su, F. J. Walker, C. H. Ahn, *APL Mater.* **2015**, *3*, 036104.
- [25] H. Zhang, Y. Yun, X. Zhang, H. Zhang, Y. Ma, X. Yan, F. Wang, G. Li, R. Li, T. Khan, Y. Chen, W. Liu, F. Hu, B. Liu, B. Shen, W. Han, J. Sun, *Phys. Rev. Lett.* **2018**, *121*, 116803.
- [26] S. Qi, H. Zhang, J. Zhang, Y. Gan, X. Chen, B. Shen, Y. Chen, Y. Chen, J. Sun, *Adv. Mater. Interfaces* **2022**, *9*, 2200103.
- [27] H. Uwe, T. Sakudo, H. Yamaguchi, *Jpn. J. Appl. Phys.* **1985**, *24*, 519.
- [28] H. Uwe, K. Oka, H. Unoki, T. Sakudo, *J. Phys. Soc. Jpn.* **1980**, *49*, 577.
- [29] C. Liu, X. Yan, D. Jin, Y. Ma, H.-W. Hsiao, Y. Lin, T. M. Bretz-Sullivan, X. Zhou, J. Pearson, B. Fisher, J. S. Jiang, W. Han, J.-M. Zuo, J. Wen, D. D. Fong, J. Sun, H. Zhou, A. Bhattacharya, *Science* **2021**, *371*, 716.
- [30] Z. Chen, Y. Liu, H. Zhang, Z. Liu, H. Tian, Y. Sun, M. Zhang, Y. Zhou, J. Sun, Y. Xie, *Science* **2021**, *372*, 721.
- [31] P. D. Eerkes, W. G. van der Wiel, H. Hilgenkamp, *Appl. Phys. Lett.* **2013**, *103*, 201603.
- [32] H. Yan, S. Zeng, K. Rubi, G. J. Omar, Z. Zhang, M. Goiran, W. Escoffier, A. Ariando, *Adv. Mater. Interfaces* **2022**, *9*, 2201633.
- [33] D. Arnold, D. Fuchs, K. Wolff, R. Schäfer, *Appl. Phys. Lett.* **2019**, *115*, 122601.
- [34] A. Joshua, S. Pecker, J. Ruhman, E. Altman, S. Ilani, *Nat. Commun.* **2012**, *3*, 1129.
- [35] F. Gunkel, C. Bell, H. Inoue, B. Kim, A. G. Swartz, T. A. Merz, Y. Hikita, S. Harashima, H. K. Sato, M. Minohara, S. Hoffmann-Eifert, R. Dittmann, H. Y. Hwang, *Phys. Rev. X* **2016**, *6*, 031035.
- [36] W. Niu, Y. Gan, Z. Wu, X. Zhang, Y. Wang, Y. Chen, L. Wang, Y. Xu, L. He, Y. Pu, X. Wang, *Adv. Mater. Interfaces* **2021**, *8*, 2101235.
- [37] P. Ghising, D. Das, S. Das, Z. Hossain, *J. Phys. Condens. Matter* **2018**, *30*, 285002.
- [38] N. W. Ashcroft, N. D. Mermin, *Solid State Physics*, Dryden Press **1976**.
- [39] K. Gopinadhan, A. Annadi, Y. Kim, A. Srivastava, B. Kumar, J. Chen, J. M. D. Coey, . Ariando, T. Venkatesan, *Adv. Electron. Mater.* **2015**, *1*, 1500114.
- [40] P. K. Rout, E. Maniv, Y. Dagan, *Phys. Rev. Lett.* **2017**, *119*, 237002.
- [41] W. Niu, Y. Zhang, Y. Gan, D. V. Christensen, M. V. Soosten, E. J. Garcia-Suarez, A. Riisager, X. Wang, Y. Xu, R. Zhang, N. Pryds, Y. Chen, *Nano Lett.* **2017**, *17*, 6878.
- [42] L. Cheng, L. Wei, H. Liang, Y. Yan, G. Cheng, M. Lv, T. Lin, T. Kang, G. Yu, J. Chu, Z. Zhang, C. Zeng, *Nano Lett.* **2017**, *17*, 6534.